4-27-2021

A Tail's Tale: Biomechanical Roles Of Dorsal Thoracic Spine Of Barnacle Nauplii

Emily Branam , '21

J. Y. Wong

B. K. K. Chan

Kit Yu Karen Chan
Swarthmore College, kchan1@swarthmore.edu

A tail's tale: Biomechanical roles of dorsal thoracic spine of barnacle nauplii

E. N. Branam [1,†], J. Y. Wong, [2,3,†], B. K. K. Chan [2] and K. Y. K. Chan[1,*]

[1] Department of Biology, Swarthmore College, Swarthmore, PA 19081, USA;

[2] Biodiversity Research Center, Academia Sinica, Taipei 11529, Taiwan

[3] Department of Life Science, National Taiwan Normal University, Taipei 11677, Taiwan;

[†] Co-first authors

[*] Corresponding author. E-mail: kchan1@swarthmore.edu; 610-328-8051(Phone); 610-328-8663(Fax)

Running Header: Biomechanics of nauplii dorsal spine

Word Count: 4499

Abstract

Many marine invertebrates have complex life histories that begin with a planktonic larval stage. Similar to other plankton, these larval invertebrates often possess protruding body extensions, but their function beyond predator deterrence is not well-documented. For example, the planktonic nauplii of crustaceans have spines. Using the epibiotic pedunculate barnacle *Octolasmis spp.*, we investigated how the dorsal thoracic spine affects swimming and fluid disturbance by comparing nauplii with their spines partially removed against those with intact spines. Our motion analysis showed that amputated *Octolasmis spp.* swam slower, in jerkier trajectories, and were less efficient per stroke cycle than those with intact spines. Amputees showed alterations in limb beat pattern: larger beat amplitude, increased phase lag, and reduced contralateral symmetry. These changes might partially help increase propulsive force generation and streamline the flow, but were insufficient to restore full function. Particle image velocimetry further showed that amputees had a larger relative area of influence, implying elevated risk by rheotactic predator. Body extensions and their interactions with limb motion play important biomechanical roles in shaping larval performance, which likely influences the evolution of form.

Keywords: functional morphology, kinematics, low Reynolds' number

Introduction

Many marine plankton possess body extensions such as spines, horns, or setae (Martin and others 2014). Various configurations of spines and other extensions in plankton can contribute towards form resistance to reduce sinking (Padisák and others 2003; Walsby and Xypolyta 1977). The size increase associated with spines can also help deter size-limited predation (Herzog and others 2016; Padisák and others 2003; Schlüter and others 1987). Operating in low to intermediate Reynold's number (*Re*), body extensions could have other biomechanical implications by changing drag force on the organisms' bodies (Koehl 1998; Koehl 1996; Wong and others 2020a). Amputation experiments remain a useful method for understanding the biomechanical roles of various structures (Delcomyn 1991; Zhang and others 2015). Focusing on the naupliar form, a common zooplankton body plan, we examined the biomechanical role of body extensions through spine removal.

Crustacean larvae make up a large proportion of planktonic biomass and play important roles as grazers and prey for higher trophic levels (Chew and others 2012; Jefferson and others 2001; Vargas and others 2006). Despite the high diversity of crustaceans, the naupliar larval form remains conserved – a form that possesses three sets of jointed swimming appendages, namely the antennules, antennae, and mandibles (Dahms 2000; Martin and others 2014; Williams 1994b). Furthermore, most nauplii have some other type of rigid body extension, e.g., the caudal spine in copepods or frontal horns and the dorsal thoracic spine in barnacles (Martin and others 2014). Understanding how these morphological features impact ecological functions could shed light on the evolution of this widespread form.

With typical sizes ranging from approximately 100 to 1000 μm and swimming speeds of 0.1-10 mm s^{-1}, most nauplii operate in low to intermediate *Re* where viscous forces dominate (Purcell 1977; Wong and others 2018). Due to the laminar nature of low *Re* environments, reciprocal motion does not lead to net displacement (Purcell 1977). The tail to head metachronal wave pattern displayed by multi-legged crustaceans is deemed the "biomechanically optimal stroke pattern" for achieving forward net displacement (Hayashi and Takagi 2020; Murphy and others 2011; Takagi 2015; Zhang and others 2014).

Another way to break reciprocal motion is to change the effective area for propulsion between strokes, which can be achieved by fanning out the setae on the tips of their appendages during the power stroke and collapsing them into bundles during the recovery stroke (Koehl 1998; Lamont and Emlet 2018; von Dassow and Emlet 2020). Non-collapsible body extensions, such as spines and horns, can also affect the overall cross-sectional area of an individual, and thus, affect the amount of drag experienced.

In addition to non-mobile morphological features, e.g., setae and spines, limb kinematics also influence swimming performance. For instance, krill achieve higher swimming speeds by increasing their pleopod beat frequency (Swadling and others 2005). Increases in stroke amplitudes also increase net forward displacement (Lenz and others 2015; Murphy and others 2011) . Given that krill have multiple pairs of limbs, limb coordination can lead to different swimming behaviors, such as hovering and fast forward motion (Ford and Santhanakrishnan 2020). For individuals with limbs that can be moved radially, body rotation can be instigated by limb pronation or supination as well as breaking contralateral (left-right) limb beat symmetry (Niimoto and others 2020). Furthermore, many crustaceans, such as mysids, krill, and branchiopod nauplii, possess non-rigid appendages that can be flexed during the recovery stroke to minimize drag (Hessler 1985; Johnson and Tarling 2008). The flexible nature and the optimal bending range of appendages for propulsion is highly conserved across taxa from small plankton to large mammals (Lucas and others 2014). Despite the ubiquity of body extensions among zooplankton, the ways in which they influence limb kinematics and the implications of their interactions for swimming are largely unknown.

Aside from whole body displacement, limb kinematic differences also impact how fluid flows around the organism's body (Jiang and others 2002a; Jiang and others 2002b). This fluid flow is crucial for delivering food particle laden water to feeding areas and can emit signals to rheotactic predators (Jiang and Kiørboe 2011; Kiørboe and others 2010). Body extensions such as horns and spines can increase the effective cross sectional area of the organisms and/or act as tethers to further direct flow for suspension feeding (Emlet and others 1985; Vogel 1988; Wong and others 2020a). Recent comparison between

feeding and non-feeding barnacle nauplii suggests that loss of feeding favors morphological change as well as limb kinematics that favor more efficient and stealthier swimming (Wong et al., 2020a). Taking into account the biomechanical roles of body extensions on key ecological functions, such as feeding and predator avoidance, could help us better understand the diversification of naupliar form.

Despite being strongly conserved as a general form across crustaceans, the nauplius exhibits many variations in the details of its morphologies, making them a useful case study for analyzing the role of body extensions (Martin and others 2014; Wong and others 2018). Barnacles in the family Lepadidae and Poecilasmatidae have very long dorsal thoracic spines and frontal horns when compared to other sessilian families (Wong and others 2018). Here, we use *Octolasmis*, a genus of epibiotic barnacle living on the gills of decapods that exists at a morphological extreme, possessing a narrow head shield and long body extensions, to determine the role of the dorsal thoracic spine in locomotion. To quantify the potential effects of dorsal thoracic spines on swimming and fluid disturbance, we used video motion analysis, limb tracking, and particle image velocimetry to compare the kinematics and hydrodynamics of freely swimming nauplii with their dorsal thoracic spine intact and 50% of the dorsal thoracic spine surgically removed.

Materials and methods

Adult collection and larval culturing

The crab *Portunus sanguinolentus* was procured from a wet market in Keelung City, Taiwan. Adult *Octolasmis cor* were cut from the gills and the epibiotic *O. warwickii* were excised from the carapace. The adult barnacles were kept in 0.45μm filtered seawater (FSW) and fed with newly hatched *Artemia* sp. *ad libitum* until the release of larvae. The newly released stage I nauplii were transferred to FSW at 34 psu and kept at room temperature (~ 25℃). Stage II individuals were randomly divided into control and cut treatment groups, hereafter amputees (Fig. 1). Half of the dorsal thoracic spine of the amputees was

removed lengthwise with custom-made ultra-fine needles and micro-scalpels from tungsten wire and glass pipette, respectively, with the methods in Wong (2020). These individuals were observed with two distinct motion analysis setups at an individual – (field of view ~ 2 x 2 mm for *O. warwickii*) and at a population scale (field of view 30 x 30 mm for *O. cor*).

Population scale observations on free swimming nauplii

Stage II *O. cor* nauplii were placed within 25 mL cell culture flasks immersed in a 25x25x25 cm recirculating water bath kept at a temperature of 25° C. Larvae were kept in 34 psu FSW, illuminated by 850nm infrared light, and filmed at 20 fps with an industrial GigE camera (GS132, Vezutech, Ltd.) fitted with a 35-80mm zoom lens at a resolution of 1280x1024 pixels. Swimming behavior of the nauplii was recorded for 6-7 minutes. New nauplii were used for each of the four replicates for each treatment. Edges of tanks were masked, and backgrounds were subtracted from each video with FOSICA (Wallingford Imaging Ltd). Subsequent analysis was performed with the in-house Matlab program Tracker3D. Smoothing splines were applied to the resulting trajectories to remove frame rate noise and to detect overall direction of travel. For each path, the following metrics were computed: 1) path duration, 2) gross speed (the first derivative of the smoothing spline), 3) net speed (the straight-line distance between start and end of a path divided by path duration), 4) net horizontal velocity ($U_{free\ swim}$), 5) net vertical velocity ($V_{free\ swim}$), 6) number of crossings across a mid-line approximating smoothing spline, 7) and average crossing distance. "Crossings" were defined as points where an individual path crossed its respective mid-line approximating smoothing spline (Fig. 2).

Individual scale observations on free swimming nauplii

The setup of high-speed video followed Chan et. al. (2013) and Gemmell et. al. (2014). *Octolasmis warwickii* nauplii were recorded in a 25 x 75 x 5 mm glass cuvette with a FastCam Mini UX100 (Photron Ltd.) fitted with a bellows and a 60mm focal length lens at 2000 frames s^{-1} at 1280 x 1024 pixels (Wong and others 2020a). Larvae were placed in a dark room and kept at 25°C using a larger buffer tank (400 mL). To trace fluid flow, the cuvettes were seeded with *Isochrysis galbana* (T-iso). Thirty individuals were used in each video session. All analyzed videos were taken from the dorsal/ventral view (xy plane).

Larval limb tracking

Larval limb positions were tracked across a complete stroke cycle for each individual at every 20th frame. The beginning of the power stroke was the time point in which the antennae were in their most rostrally-extended positions. The appendages on both the left and right side of the nauplii were tracked. The tip of each appendage (antennule, antennae, and mandible) was defined as the point at which the appendage ended and the setae began, Landmarking was performed with tpsDIG2 (version 2.31). To track the positioning of limbs in relation to the body, a body centroid was calculated from three body landmarks – the tip of the left horn, right horn, and dorsal thoracic spine. For amputees, the third body landmark was placed at the point at which the spine was cut, reflecting the potential shift in center of mass (Fig. 1). Larvae displaying morphological abnormalities (bent tail or horns) were excluded from the limb kinematic analysis; ten amputated nauplii videos and nine control nauplii were compared.

The limb beat angle θ of a given appendage was the angle between the vector $\overrightarrow{CA}$ (centroid to appendage tip) and $\overrightarrow{CT}$ (centroid to dorsal thoracic spine tip). Angular separation between limb pairs on the left or right side of the body was calculated as a proxy for phase lag at four time points: start of power stroke, mid power stroke, end of power stroke/start of recovery stroke, and mid recovery stroke. These time points were determined based on the limb beat angles of the right antennae because this pair of limbs

was the major contributor to nauplii movement (Wong and others 2020a). To test for contralateral symmetry in limb beats, we subtracted the limb beat angle of the right from the left. Whole larval movement was quantified with net displacement normalized with body length and forward to backward displacement ratio. Limb beat frequency was calculated based on the stroke duration.

Additionally, we tracked the flexion point and flexion ratio of the antennae across stroke cycle after Lucas et. al. (2014). The flexion point was defined as the point of maximum curvature (Fig. 1). In instances of straight extensions, the tip of the appendage was marked as the flexion point. The angle of flexion (φ) was calculated as the dot product of the vectors from the flexion point to the body centroid $\overrightarrow{CI}$ and from the flexion point to antenna tip $\overrightarrow{CP}$.The inflection ratio was the $|\overrightarrow{CI}|$ divided by the sum of$|\overrightarrow{CI}|$ and$|\overrightarrow{CP}|$.

Flow field analysis

Particle image velocimetry analysis followed Wong and others (2020a). Using the software DaVis (version 8.2.1, LaVision GmbH), we visualized flow fields of each nauplius. Nauplii were masked algorithmically (smoothing, sliding maximum, and sliding minimum subtractions), followed by thresholding. Cross correlation computation on instantaneous velocity vectors was achieved using a multi-pass algorithm with decreasing interrogation window size from 64 x 64 to 32 x 32 pixels with 50% overlaps. Vector post processing removed outlier vectors. Final velocity vectors V_{flow} were exported as 80 x 64 cell grids for spatial attenuation and flux calculations (each cell represents 16 x 16 pixels with (u,v) components representing velocity in the (x,y) directions). Flow fields around five representative individuals from each treatment group were compared.

Spatial attenuation of the flow (n), a factor that can influence detection by predators, was computed after Kiørboe and others (2014), where

$$\| V_{flow} \| \propto r^n.$$

Binning of flow speed was performed with different thresholds U^*, and r (magnitude of the spatial extent of flow) was determined as the radius of the circle of area equivalent to the area encompassed by binned speed (U^*). A power law fitting was used to estimate n as the slope of the regression.

Our earlier work showed flow towards the feeding area occurred during the recovery stroke (Wong et al., 2020a), thus, we computed the volume of fluid passing through a line segment (l) when the backwards velocity was largest. Given that the body centroid shifted with the amputation but the location of feeding region (labrum) did not, for a more accurate comparison, we defined the center of the head shield (C') using the landmarks of the horns and the posterior end of the head shield (P) where the dorsal thoracic spine protrudes (Fig. 1). The flux line was placed perpendicular to the vector $\overrightarrow{C'P}$ and centered at three $\overrightarrow{C'P}$ away from C'. To obtain a 2D estimate of the flux, we defined the length of the flux line to be $2 \times |\overrightarrow{C'P}|$, which roughly corresponded to the length of the head shield. The approximation of flux, ϕ, was calculated by taking the sum of the magnitude of velocity vectors projected on normal direction and multiplying it by velocity vector length

$$\phi_{x,y} = \sum(u,v) \cdot n \, \mathrm{d}l.$$

n represents the normal unit vector, and the dot product provides the magnitude of velocity vector projected onto the normal direction. Relative flux accounting for the nauplii velocity was calculated.

Statistical analysis

All statistical analyses were performed in R (version 3.6.2). Because multiple videos of each treatment were used for replication in the population level observation, we first checked for significance of a video identity for the video motion analysis using a Linear Mixed Effect Model with treatment categorized as a fixed effect and video identity (replication) as a random effect. Once we confirmed that video identity did

not significantly affect the metric of interest, we removed that factor and compare swimming with a t-test. Normality and homogeneity of variance were checked with Q-Q plot and F test, respectively. Given the small sample size of the kinematic and flow field observations, we tested for the effect of amputation on those metrics with permutation F-tests (1000 Permutations).

Results

Behavior of population scale freely swimming larvae

Treatment had significant effects on five of the seven metrics: Gross speed ($t_{1, 435} = 7.56$, $p < 0.001$), net speed ($t_{1, 435} = 6.03$, $p < 0.001$), net $V_{\text{free swim}}$ ($t_{1, 435} = -2.89$, $p = 0.004$), number of crossings ($t_{1, 435} = -4.27$, $p < 0.001$), and average crossing distance ($t_{1, 435} = 7.23$, $p < 0.001$, Fig. 2). In the control group, *O. cor* nauplii had mean gross speed 37.4% higher (observed difference: 0.2 mm s^{-1}) and mean net speed 53.9% higher (0.13 mm s^{-1}) than the amputees. Net *V* was significantly lower in control *O. cor* by an average of -6.6% (0.08 mm s^{-1}). There were significantly fewer crossings, spaced farther away in control *O. cor,* suggesting less convoluted paths (37.9 crossings in control compared to 58.3 crossings in amputated; 0.355 mm crossing distance in control compared to 0.229 mm in amputated).

Individual swimming kinematics

A 26.2% decrease in normalized speed was observed in *O. warwickii* amputees when compared to controls (Fig. 3, Table 1). Forward: backward displacement ratio was lower in amputees by 38.9%. Amputated nauplii also displayed a lowered limb beat frequency by 8.8% (Table 1). Both treatment groups operated in *Re* near unity (1.83±0.45 and 0.74±0.37 for control and amputee, respectively). Significant differences in angular separation between the two treatment groups were also found across all but one time point and limb pair. The exception was the start of the power stroke between the antennule

and antenna for both the left and right sides (Suppl. Table 1). Regarding limb beat symmetry, the difference between left and right mandible beat angle of amputees was 81.6% greater than control nauplii during mid-power stroke (Fig. 3). Amputees beat their limbs at significantly greater amplitudes than controls for all appendages but the right-side antennule. (Table 1). Additionally, amputees straightened both antennae at the end of the power stroke more than controls. The flexion angle of amputees' antennae at the end of the power stroke was > 50% smaller than the control for both the left and the right (Table 1). The flexion ratio also differed between treatments across multiple time points, with flexion occurring closer to the larval body among amputees (Suppl. Fig. 1; Table 1).

Particle Image Velocimetry

While the differences in spatial attenuation displayed statistical significance between the two treatments, they were of the same order of 1 ($F_{1, 8} = 4.98$, $p = 0.005$, Fig. 4). The area of influence, i.e., area with flow velocity greater than the 80th percentile of all recorded velocity, were on average not different between the control and amputee ($F_{1, 8} = 0.432$, $p = 0.5$). However, when normalized by the square of body length, the amputees created a ~3 fold larger fluid disturbance (Fig. 4, $F_{1,8} = 12.4$, $p < 0.001$) The average relative flux for the amputee when body backward velocity was largest was comparable to that of the control ($F_{1, 8} = 1.35$, $p = 0.289$). However, the results were highly variable between individuals with the standard deviations of 0.49 mm^2 s^{-1} for the control compared to 1.30 mm^2 s^{-1} for the amputated group (Fig. 4).

Discussion

Many planktonic organisms, including highly mobile natatory forms, have long body extensions suggesting that functions beyond anti-predation are likely. Using stage II barnacle nauplii from the genus *Octolasmis* that possess an extremely long dorsal thoracic spine relative to their size and to other barnacles, we investigated the biomechanical role of this body structure. Our observations highlighted

that body extensions enhanced swimming proficiency and reduced predation risk. When the body extension was experimentally reduced in length, possibly compensatory changes in limb kinematics were observed: increased stroke amplitude and limb-limb angular separation to generate larger propulsive force as well as reduced flexion angle at the beginning of the recovery stroke for streamlining. However, these changes were not sufficient to compensate for the reduction of the spine. These observations highlight how the interactions between rigid morphological structures, e.g., spines, and moving limbs, shape key ecological functions of multi-legged swimmers.

Spine damage compromises swimming

Freely-swimming, amputated *Octolasmis cor* nauplii were observed to have lower net and gross speeds and "jerkier" swimming trajectories with higher numbers of crossings along the mid-line that were more closely spaced (Fig. 2). The observed swimming speed reduction was reiterated among *O. warwickii* nauplii tracked with high-speed videography (Fig. 3). These observed differences between treatment groups were unlikely due to handling stress since both amputated and control nauplii were manipulated with a probe. Indeed, the change in swimming speed and overall trajectories were likely associated with the change in limb kinematics discussed below.

Loss of spine and reduction in swimming speed have functional implications, particularly for predator avoidance. The amputation could be interpreted as a proxy for injuries sustained during partial predation observed in nature (Elliott and Tang 2011; Ohman 1984). That spines assist in size deterrence is well-documented among plankton (Herzog and others 2016; Schlüter and others 1987). Given that the *Octolasmis* nauplii we studied underwent a decrease in size of >400 μm (~40% of body length), an order of magnitude larger than the previously reported induced anti-predation responses, vulnerability to size-limited predators likely increased with spine length reduction. Some barnacle nauplii undertake diel vertical migrations, and a reduction of swimming speed could compromise the organisms' ability to keep

speed with light attenuation rates (Bonicelli and others 2016; Richards and others 1996). Therefore, injuries incurred on body extensions could negatively affect survivorship.

Changes in limb kinematics

The observed reduction in swimming performance was accompanied by several changes in limb kinematics. First, amputees displayed higher limb beat amplitudes than controls. Numerical models of planktonic crustaceans suggested that increases in limb beat amplitude increase net displacement per stroke cycle until eventually plateauing due to limb interactions (Lenz and others 2015; Takagi 2015). Second, the flexion angles of the antennae were smaller among amputated nauplii at the end of the power stroke, i.e., straighter limbs, than controls. We focused on the antennae because they are generally the main propulsors in crustacean nauplii, and the mandibles are reduced and their activities harder to quantify (Gauld 1959; Moyse 1984; Williams 1994a). Swimming pteropods and the nauplii of other crustaceans at comparable *Re* are observed to orient their wings or limbs parallel to flow to minimize drag (Hessler 1985; Johnson and Tarling 2008). The observed reduction in flexion angle at the end of the power stroke might also contribute towards amputees' forward motion. It is important to note that in addition to streamlining, these flexible limbs were also effective thrust generating propulsors: the flexion angles at the beginning of the power stroke were 19.5 ^{o} and 25.6 ^{o} for control and amputated nauplii, matching the universal optimal range of maximum propulsor flexion angle (Lucas and others 2014). These two kinematic adjustments (increased amplitude and decreased curvature) may act in conjunction to partially compensate for the loss of the spine. However, it is important to note that with a $Re \approx 1$, streamlining during recovery stroke translated into further backward displacement. As a result, the amputees were less efficient at swimming forward per stroke cycle.

A third change in limb kinematics was the increased phase lag between pairs of limbs when spines were amputated. Previous comparisons between planktotrophic and lecithotrophic barnacle nauplii

suggested that anti-phase beating of the appendages provided additional anchoring effects and helped direct food particles towards the food capture area (Wong and others 2020a). For *O. warwickii*, we observed that at the end of the recovery stroke, due to the larger angular separation, antenna and mandible moved in opposite directions, and on occasion, touched each other (Fig. 3, Table 1). A large phase lag and the resulting limb-limb interactions were shown to reduce net displacement in copepods and krill (Ford and Santhanakrishnan 2020; Ford and others 2019; Lenz and others 2015). Perhaps the increased phase lag observed helps dampen the backward displacement during recovery stroke after spine removal.

The fourth and final change in kinematics was the shift in contralateral synchrony, i.e., the asynchronous beating of the left and right pairs of appendages (Fig. 3, Table 1). For copepod nauplii, yaw occurred as a result of pronation or supination of the antenna such that one side drove more fluid motion than the other (Niimoto and others 2020). We observed a significant change in mandible symmetry during mid-power stroke in amputated nauplii, which likely translated into yaw. Partial removal of the dorsal thoracic spine not only reduced form drag, but also likely influenced weight distribution and stability, i.e., the ability to maintain directed motion (Grünbaum and Strathmann 2003). The observed behaviors associated with body rotation could possibly be another form of (partial) compensation, and the mechanosensory feedback that underlies such behaviors warrants further investigation.

Change in velocity field

The observed differences in overall morphology and limb kinematics led to a shift in flow field around the nauplii such that amputees had a larger normalized area of influence (Fig. 4). The risk of predation by rheotactic predator is proportional to this fluid signal (Kiørboe and others 2014). Hence, it is reasonable to predict that loss of spine increases predation risk, which agrees with the field observations that dead copepod nauplii are often partially consumed (Elliott and Tang 2011). The average spatial attenuation (n) of both groups was ~1 (Table 1), which was comparable to values observed for the planktonic nauplii of

Tetraclita japonica and *Capitulum mitella* (Wong and others 2020a; Wong and others 2020b). Compared to an $n \approx 3$ for the lecithotrophic *Polyascus planus*, the extremely long dorsal thoracic spine of *Octolasmis* did not appear to aid in flow attenuation. Delivery of food laden water to the labrum, and thus, feeding efficiency is determined by the flux, i.e. velocity of water per unit area. The measured relative flux towards the labrum remained comparable between amputee and the control. This lack of difference was likely due to the fact that relative flux towards the larval body was mostly attributed to body motion, which was an order of magnitude larger than the flow induced by the beating appendages (here and (Andersen and Kiørboe 2020; Wong and others 2020a)). However, the relative flux was more variable among amputated individuals, which could still imply reduction in time-integrated clearance. Vorticity and particle tracking velocimetry studies could confirm these two proposed reductions in ecological functions by detailing the viscous vortex ring structures and testing whether particles enter the labrum.

Body extensions of zooplankton are not only rigid structures for predator deterrence and buoyancy regulation. Our observations on barnacle nauplii with extremely long dorsal thoracic spine showed that these extensions also interact with the flexible beating appendages to affect swimming speed and the size-normalized flow disturbance around an individual. Nevertheless, this interaction could become more important through ontogeny as the dorsal thoracic spine lengthens and appendage setations become more complicated. For small plankton operating in low to intermediate *Re*, these changes in flow field in turn shape their abilities to capture food particles and avoid predation. The biomechanical and behavioral constraints associated with these limb-spine interactions likely influenced the evolution and diversification of crustacean naupliar form.

Acknowledgments

We acknowledge D. Tong, E. Wong, H. Tso, Y. K. Tam and P.C. Tsoi for technical support and W.H. Ko for analysis assistance. Funding of this project was provided by the Ministry of Science and Technology, Taiwan (106-2923-B-001-002-MY3 to BC). The Croucher Foundation and Faculty Research Fund from Swarthmore College supported KC. JW was supported by a TIGP PhD Fellowship.

Data availability statement

The data unerlying this article is available at https://osf.io/sg5a8/.

Figure captions

Figure 1

Nauplii in the two treatment groups, (A) control and (B) amputated, showing landmarks used for kinematics analysis; Fh, Frontal horn; Dts, Dorsal thoracic spine; XDts, Amputated dorsal thoracic spine, P, posterior point on head shield, C', head shield centroid. AP indicates the location of the abdominal process. Black lines indicate vectors from body centroid to appendage tips ($\overrightarrow{CA}$) and body centroid to tip of dorsal thoracic spine ($\overrightarrow{CP}$) for calculating limb angle, and vectors from centroid to point of maximum antenna curvature and curvature point to antenna tip for calculating flexion angle and ratio. Line for flux calculation is $3\left|\overrightarrow{C'P}\right|$ from C'.

Figure 2. Population-level observation of freely swimming *Octolasmis cor* nauplii (A-F, 267 and 170 trajectories for control and amputees, respectively). All boxplots compare control treatment (white) with amputated treatment (grey). Each box represents the 1st and 3rd quartiles with maximum and minimum values represented by extended lines perpendicular to the box. Mean value is represented by the line within each box. $p < 0.001$ is marked by asterisks (***). Swimming trajectory in grey and smoothing spline along the midline in black and "crossings" are marked with black crosses (G). Representative example swimming trajectories of control (H) and amputated nauplii (I).

Figure 3 Limb angle of control (A, B) and amputated (D, E) *Octolasmis warwickii* nauplii through one beat cycle. All 3 pairs of appendages (ant1:antennule, ant2: antenna, mand: mandible) on both the left and right were tracked . Vertical light grey lines denote the start of power stroke (PS), mid power stroke (MPS), start of recovery stroke (RS), and mid recovery stroke (MRS). Control larvae had higher net displacement (C, F) and forward : backward ratio than the amputees (J). Amputated nauplii had larger limb beat angle (G) and angular separation between limb pairs (H); only data on the left is shown. Largest difference in asymmetry between the left and the right pairs of limbs was recorded for the mandible during mid power stroke (I). See Fig. 2 for the details of the boxplots and * indicates $p < 0.05$,** indicates $p < 0.01$, *** indicates $p < 0.001$.

Figure 4. Flow field around representative nauplii with spine intact (A) and amputated (B) at the moment of maximum body backward displacement in a stroke cycle. Open squares mark the head shield centroid, open circles mark the midpoint of the flux line (black). The area of influence was normalized by squared body-length and was found to be significantly higher for amputees (C), but the relative flux was comparable between the two groups after accounting for body velocity (D). ** indicates $p < 0.01$

References

Andersen A, Kiørboe T. 2020. The effect of tethering on the clearance rate of suspension-feeding plankton. Proceedings of the National Academy of Sciences 117:30101-30103.

Bonicelli J, Tyburczy J, Tapia FJ, Finke GR, Parragué M, Dudas S, Menge BA, Navarrete SA. 2016. Diel vertical migration and cross-shore distribution of barnacle and bivalve larvae in the central Chile inner-shelf. Journal of Experimental Marine Biology and Ecology 485:35-46.

Chan KYK, Jiang H, Padilla DK. 2013. Swimming speed of larval snail does not correlate with size and ciliary beat frequency. PloS one 8:e82764.

Chew LL, Chong VC, Tanaka K, Sasekumar A. 2012. Phytoplankton fuel the energy flow from zooplankton to small nekton in turbid mangrove waters. Marine Ecology Progress Series 469:7-24.

Dahms H-U. 2000. Phylogenetic implications of the crustacean nauplius. Hydrobiologia 417:91-99.

Delcomyn F. 1991. Perturbation of the motor system in freely walking cockroaches. I. Rear leg amputation and the timing of motor activity in leg muscles. Journal of experimental Biology 156:483-502.

Elliott DT, Tang KW. 2011. Spatial and temporal distributions of live and dead copepods in the lower Chesapeake Bay (Virginia, USA). Estuaries and Coasts 34:1039-1048.

Emlet R, Strathman R, Strickler J. 1985. Gravity, drag, and feeding currents of small zooplankton. Science 228:1016-1017.

Ford M, Santhanakrishnan A. 2020. On the role of phase lag in multi-appendage metachronal swimming of euphausiids. Bioinspiration & Biomimetics.

Ford MP, Lai HK, Samaee M, Santhanakrishnan A. 2019. Hydrodynamics of metachronal paddling: effects of varying Reynolds number and phase lag. Royal Society Open Science 6:191387.

Gauld D. 1959. Swimming and feeding in crustacean larvae: the nauplius larva. Proceedings of the Zoological Society of London 132:31-50.

Gemmell BJ, Jiang H, Buskey EJ. 2014. A new approach to micro-scale particle image velocimetry (μPIV) for quantifying flows around free-swimming zooplankton. Journal of Plankton Research 36:1396-1401.

Grünbaum D, Strathmann RR. 2003. Form, performance and trade-offs in swimming and stability of armed larvae. Journal of Marine Research 61:659-691.

Hayashi R, Takagi D. 2020. Metachronal swimming with rigid arms near boundaries. Fluids 5:24.

Herzog Q, Tittgen C, Laforsch C. 2016. Predator-specific reversibility of morphological defenses in *Daphnia barbata*. Journal of Plankton Research 38:771-780.

Hessler RR. 1985. Swimming in Crustacea. Earth and Environmental Science Transactions of The Royal Society of Edinburgh 76:115-122.

Jefferson TT, Henrik L, Torkel Gissel N, Benni Winding H. 2001. Zooplankton feeding ecology: grazing on phytoplankton and predation on protozoans by copepod and barnacle nauplii in Disko Bay, West Greenland. Marine Ecology Progress Series 221:209-219.

Jiang H, Kiørboe T. 2011. The fluid dynamics of swimming by jumping in copepods. Journal of the Royal Society Interface 8:1090-1103.

Jiang H, Meneveau C, Osborn TR. 2002a. The flow field around a freely swimming copepod in steady motion. Part II: Numerical simulation. Journal of Plankton Research 24:191-213.

Jiang H, Osborn TR, Meneveau C. 2002b. The flow field around a freely swimming copepod in steady motion. Part I: Theoretical analysis. Journal of Plankton Research 24:167-189.

Johnson ML, Tarling GA. 2008. Influence of individual state on swimming capacity and behaviour of Antarctic krill *Euphausia superba*. Marine Ecology Progress Series 366:99-110.

Kiørboe T, Jiang H, Colin SP. 2010. Danger of zooplankton feeding: the fluid signal generated by ambush-feeding copepods. Proceedings of the Royal Society B: Biological Sciences 277:3229-3237.

Kiørboe T, Jiang H, Gonçalves RJ, Nielsen LT, Wadhwa N. 2014. Flow disturbances generated by feeding and swimming zooplankton. Proceedings of the National Academy of Sciences 111:11738-11743.

Koehl M. 1998. Small-scale hydrodynamics of feeding appendages of marine animals. Oceanography 11:10-12.

Koehl MAR. 1996. When does morphology matter? Annual Review of Ecology and Systematics 27:501-542.

Lamont EI, Emlet RB. 2018. Permanently fused setules create unusual folding fans used for swimming in cyprid larvae of barnacles. Biological Bulletin 235:185-194.

Lenz PH, Takagi D, Hartline DK. 2015. Choreographed swimming of copepod nauplii. Journal of The Royal Society Interface 12:20150776.

Lucas KN, Johnson N, Beaulieu WT, Cathcart E, Tirrell G, Colin SP, Gemmell BJ, Dabiri JO, Costello JH. 2014. Bending rules for animal propulsion. Nature communications 5:1-7.

Martin JW, Olesen J, Høeg JT, Høeg J. 2014. Atlas of crustacean larvae. JHU Press.

Moyse J. 1984. Some observations on the swimming and feeding of the nauplius larvae of *Lepas pectinata* (Cirripedia: Crustacea). Zoological journal of the Linnean Society 80:323-336.

Murphy D, Webster D, Kawaguchi S, King R, Yen J. 2011. Metachronal swimming in Antarctic krill: Gait kinematics and system design. Marine biology 158:2541-2554.

Niimoto K, Kuball KJ, Block LN, Lenz PH, Takagi D. 2020. Rotational maneuvers of copepod nauplii at low Reynolds number. Fluids 5:78.

Ohman MD. 1984. Omnivory by *Euphausia pacifica:* The role of copepod prey. Marine ecology progress series. Oldendorf 19:125-131.

Padisák J, Soróczki-Pintér É, Rezner Z. 2003. Sinking properties of some phytoplankton shapes and the relation of form resistance to morphological diversity of plankton—an experimental study. Aquatic biodiversity. Springer. p. 243-257.

Purcell EM. 1977. Life at low Reynolds number. American journal of physics 45:3-11.

Richards SA, Possingham HP, Noye J. 1996. Diel vertical migration: modelling light-mediated mechanisms. Journal of Plankton Research 18:2199-2222.

Schlüter M, Groeneweg J, Soeder CJ. 1987. Impact of rotifer grazing on population dynamics of green microalgae in high-rate ponds. Water Research 21:1293-1297.

Swadling K, Ritz D, Nicol S, Osborn J, Gurney L. 2005. Respiration rate and cost of swimming for Antarctic krill, *Euphausia superba,* in large groups in the laboratory. Marine Biology 146:1169-1175.

Takagi D. 2015. Swimming with stiff legs at low Reynolds number. Physical Review E 92:023020.

Vargas CA, ManrÍquez PH, Navarrete SA. 2006. Feeding by larvae of intertidal invertebrates: assessing their position in pelagic food webs. Ecology 87:444-457.

Vogel S. 1988. Life's Devices: The physical world of animals and plants. Princeton University Press.

von Dassow G, Emlet RB. 2020. Direct observation of the setular web that fuses thoracopodal setae of a calanoid copepod into a collapsible fan. Biological Bulletin 238:73-79.

Walsby A, Xypolyta A. 1977. The form resistance of chitan fibres attached to the cells of *Thalassiosira fluviatilis* Hustedt. British Phycological Journal 12:215-223.

Williams TA. 1994a. A model of rowing propulsion and the ontogeny of locomotion in Artemia larvae. Biological Bulletin 187:164-173.

Williams TA. 1994b. The nauplius larva of crustaceans: functional diversity and the phylotypic stage. American Zoologist 34:562-569.

Wong J, Chan BK, Chan K. 2020a. Evolution of feeding shapes swimming kinematics of barnacle naupliar larvae: a comparison between trophic modes. Integrative Organismal Biology.

Wong J, Chan BK, Chan KK. 2020b. Swimming kinematics and hydrodynamics of barnacle larvae throughout development. Proceedings of the Royal Society B 287:20201360.

Wong J, Chan KK, Chan BK. 2018. Phylogenetic, ecological and biomechanical constraints on larval form: A comparative morphological analysis of barnacle nauplii. PloS one 13:e0206973.

Wong JY. 2020. Comparative biomechanics of barnacle larvae. [Taiwan]: National Taiwan Normal University

Zhang C, Guy RD, Mulloney B, Zhang Q, Lewis TJ. 2014. Neural mechanism of optimal limb coordination in crustacean swimming. Proceedings of the National Academy of Sciences 111:13840-13845.

Zhang Y, Zhang J, Ren L. 2015. The terrestrial locomotion of a mole cricket with foreleg amputation. Science China Technological Sciences 58:999-1006.

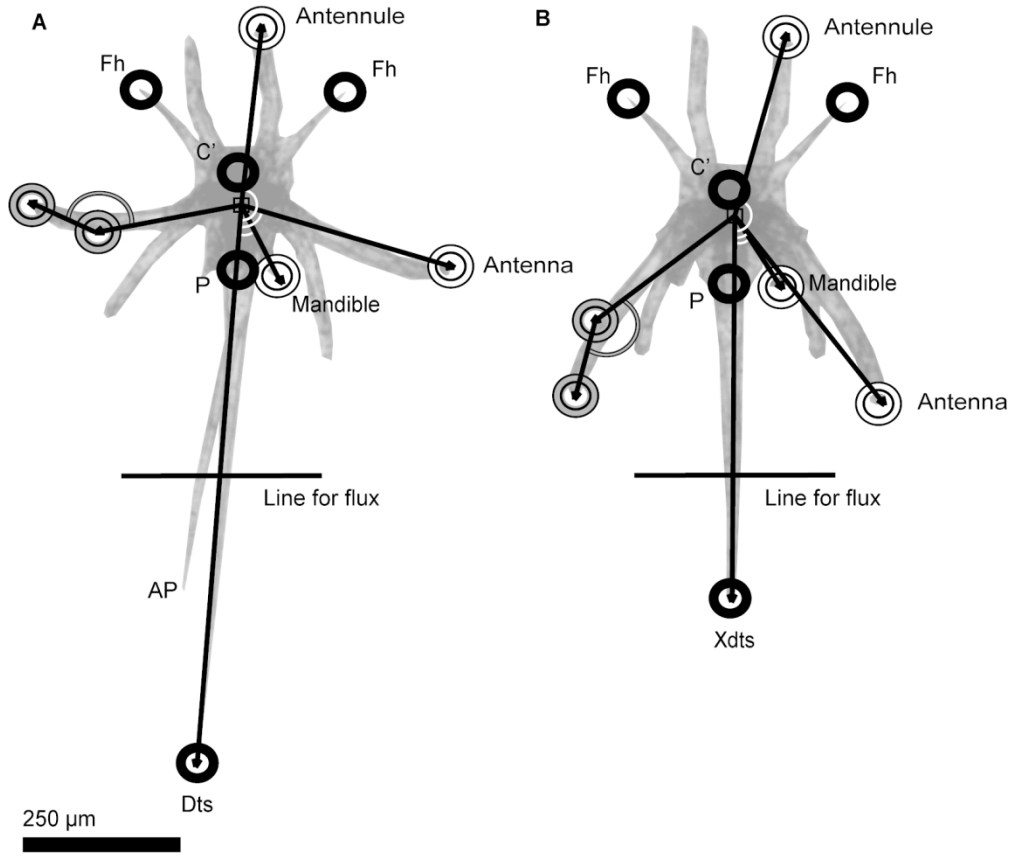

Nauplii in the two treatment groups, (A) control and (B) amputated, showing landmarks used for kinematics analysis; Fh, Frontal horn; Dts, Dorsal thoracic spine; XDts, Amputated dorsal thoracic spine, P, posterior point on head shield, C′, head shield centroid. AP indicates the location of the abdominal process. Black lines indicate vectors from body centroid to appendage tips ($(CA)^{\rightarrow}$) and body centroid to tip of dorsal thoracic spine ($(CP))^{\rightarrow}$) for calculating limb angle, and vectors from centroid to point of maximum antenna curvature and curvature point to antenna tip for calculating flexion angle and ratio. Line for flux calculation is $3|(C'P)^{\rightarrow}|$ from C′.

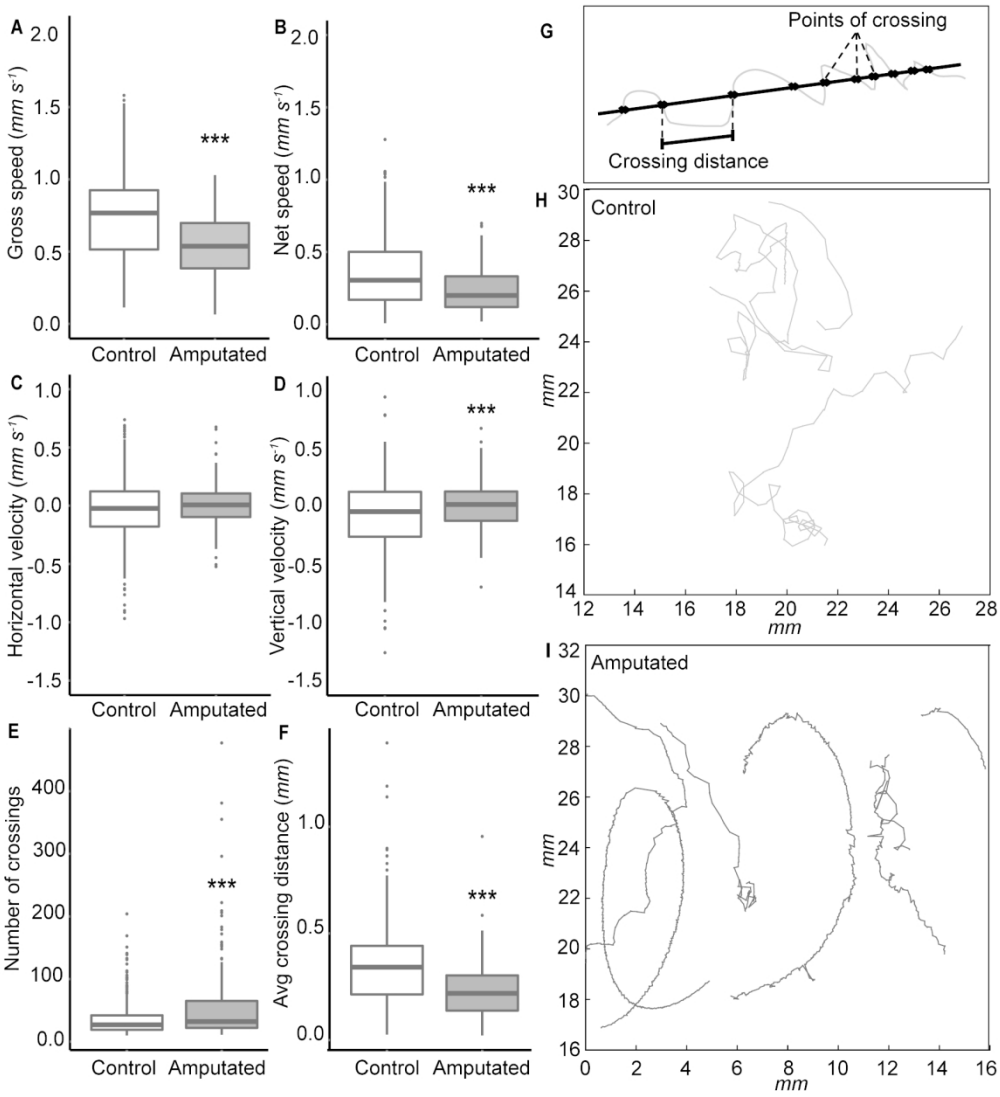

Population-level observation of freely swimming Octolasmis cor nauplii (A-F, 267 and 170 trajectories for control and amputees, respectively). All boxplots compare control treatment (white) with amputated treatment (grey). Each box represents the 1st and 3rd quartiles with maximum and minimum values represented by extended lines perpendicular to the box. Mean value is represented by the line within each box. $p < 0.001$ is marked by asterisks (***). Swimming trajectory in grey and smoothing spline along the midline in black and "crossings" are marked with black crosses (G). Representative example swimming trajectories of control (H) and amputated nauplii (I).

157x171mm (300 x 300 DPI)

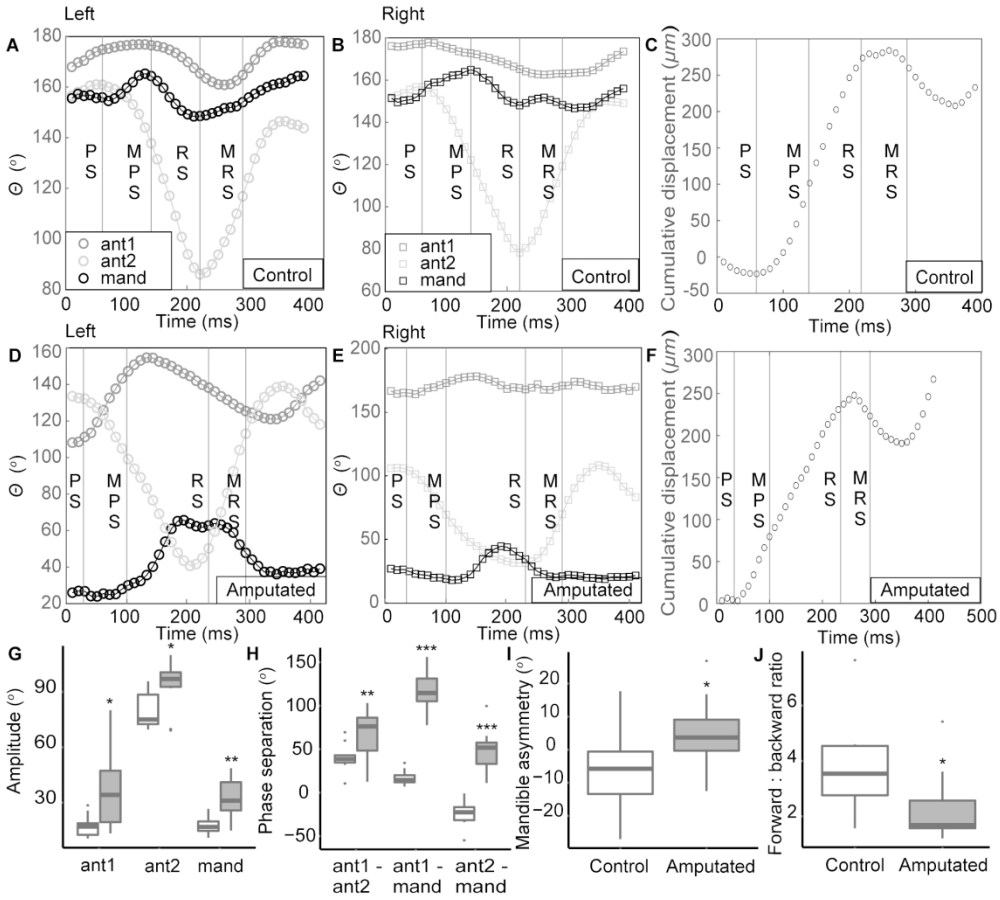

Limb angle of control (A, B) and amputated (D, E) Octolasmis warwickii nauplii through one beat cycle. All 3 pairs of appendages (ant1:antennule, ant2: antenna, mand: mandible) on both the left and right were tracked . Vertical light grey lines denote the start of power stroke (PS), mid power stroke (MPS), start of recovery stroke (RS), and mid recovery stroke (MRS). Control larvae had higher net displacement (C, F) and forward : backward ratio than the amputees (J). Amputated nauplii had larger limb beat angle (G) and angular separation between limb pairs (H); only data on the left is shown. Largest difference in asymmetry between the left and the right pairs of limbs was recorded for the mandible during mid power stroke (I). See Fig. 2 for the details of the boxplots and * indicates $p < 0.05$,** indicates $p < 0.01$, *** indicates $p < 0.001$.

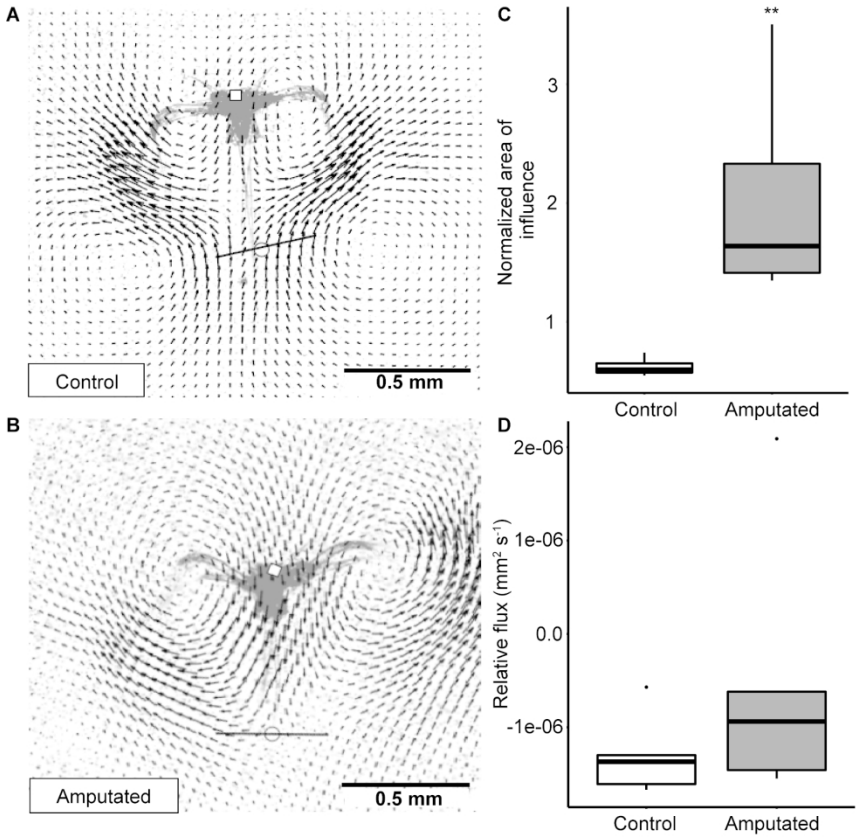

. Flow field around representative nauplii with spine intact (A) and amputated (B) at the moment of maximum body backward displacement in a stroke cycle. Open squares mark the head shield centroid, open circles mark the midpoint of the flux line (black). The area of influence was normalized by squared body-length and was found to be significantly higher for amputees (C), but the relative flux was comparable between the two groups after accounting for body velocity (D). ** indicates $p < 0.01$

161x134mm (300 x 300 DPI)

Table 1.

Limb kinematics and fluid disturbance of control and amputated *Octolasmis warwickii* nauplii. PS: start of power stroke, MPS: mid-power stroke, RS: start of recovery stroke, MRS:mid-recovery stroke. Ant1: antennule, ant2: antennae, mand: mandible. Statistically significant differences ($p<0.05$) are bold-faced.

			Control ($\bar{x}_c \pm$ SD)	Amputated ($\bar{x}_a \pm$ SD)	F	*p*
Speed (mm s^{-1})			**1.65±0.305**	**1.25±0.359**	**6.52**	**0.028**
Forward:backward displacement ratio			**3.81 ±1.72**	**2.33±1.31**	**4.52**	**0.045**
Beat frequency (Hz)			**2.53 ±0.128**	**2.31±0.123**	**15.1**	**0.004**
Asymmetry (°)	Ant1	PS:	0.879 °±8.07 °	-3.23°±25.6°	0.211	0.667
		MPS:	1.37 ° ±8.52 °	-0.518 ° ±19.8 °	0.0694	0.822
		RS:	1.34° ±6.43 °	-2.06 ° ±16.5 °	0.336	0.580
		MRS:	2.78 ° ±10.1 °	-4.82 ° ±13.9 °	1.81	0.197
	Ant2	PS:	-1.31 ° ±10.2 °	-6.19 ° ±17.7 °	0.520	0.467
		MPS:	0.900 ° ±15.6 °	-4.60 ° ±26.0 °	0.302	0.582
		RS:	1.44 ° ±11.0 °	4.63 ° ±16.6 °	0.238	0.613
		MRS:	-0.386 ° ±6.43 °	0.316 ° ±25.4 °	0.00670	0.939
	Mand	PS:	-4.17 ° ±11.1 °	0.582 ° ±14.9 °	0.615	0.448
		MPS:	**-6.56 ° ±12.7 °**	**5.36 ° ±10.8 °**	**4.87**	**0.035**
		RS:	-3.35 ° ±5.34 °	4.08 ° ±11.5 °	3.14	0.102
		MRS:	-3.28 ° ±10.4 °	3.58 ° ±8.37 °	2.54	0.144
Amplitude (°)	Left –ant1		**17.6°±6.16 °**	**36.8°±20.9 °**	**6.95**	**0.014**
	Left –ant2		**80.5°±10.2 °**	**93.5°±13.7 °**	**5.46**	**0.037**
	Left-mand		**17.5°±4.40 °**	**31.6°±11.4 °**	**12.2**	**0.002**
	Right-ant1		19.3°±5.54°	24.4°±13.7°	1.08	0.358
	Right-ant2		**80.6°±10.7°**	**95.3°±16.4°**	**5.25**	**0.045**
	Right-mand		**19.5°±6.83°**	**29.6°±7.29°**	**9.62**	**0.008**
Flexion angle (°)	Left – ant2	PS:	14.7°±11.6 °	23.2 °±11.5 °	2.54	0.117
		MPS:	31.6 °±32.3 °	48.2°±26.7°	1.50	0.225
		RS:	**108°±11.8°**	**51.0°±27.0°**	**34.3**	**0.001**
		MRS:	61.5°±42.7°	44.9°±26.7°	1.06	0.329
	Right –ant2	PS:	19.6°±14.4°	25.8°±9.26°	1.27	0.295
		MPS:	48.9°±41.3°	49.0°±23.3°	0.00	0.996
		RS:	**105°±19.4°**	**47.2°±20.2°**	**40.5**	**0.001**
		MRS:	61.4°±36.0°	45.4°±23.6°	1.34	0.258
Flexion ratio	Left – ant2	PS:	**0.837±0.071**	**0.730±0.114**	**5.88**	**0.019**
		MPS:	0.801±0.087	0.739±0.101	2.02	0.189
		RS:	0.652±0.047	0.691±0.092	1.33	0.244
		MRS:	**0.764±0.055**	**0.694±0.079**	**4.95**	**0.048**
	Right –ant2	PS:	**0.835 ±0.046**	**0.720±0.059**	**22.2**	**<0.001**
		MPS:	0.783±0.062	0.739±0.099	1.30	0.321
		RS:	0.662±0.057	0.639±0.057	0.452	0.509
		MRS:	**0.792±0.045**	**0.699±0.083**	**8.91**	**0.008**
Absolute area of influence (mm^2)			0.646±0.032	0.663±0.05	0.432	0.500
Body length^2 normalized area of influence			**0.621±0.07**	**2.05±0.90**	**4.98**	**0.005**
Spatial attenuation power (*n*)			**-1.17±0.040**	**-1.28±0.102**	**12.4**	**<0.001**
Relative flux (mm^2 s^{-1})			-1.39±0.439	0.495±1.49	1.35	0.289